# A Critical Look at Deriving Monthly Aerosol Optical Depth From Satellite Data

Robert C. Levy, Gregory G. Leptoukh, Ralph Kahn, Victor Zubko, Arun Gopalan, and Lorraine A. Remer

*Abstract*—**Satellite-derived aerosol data sets, such as those provided by NASA's Moderate Resolution Imaging Spectrora-diometer (MODIS) instruments, are greatly improving our understanding of global aerosol optical depth (AOD). Yet, there are sampling issues. MODIS' specific orbital geometry, convolved with the need to avoid bright surfaces (glint, desert, clouds, etc.), means that AOD can be under- or over-sampled in places. When deriving downstream products, such as daily or monthly gridded AOD, one must consider the spatial and temporal density of the measurements relative to the gradients of the true AOD. Additionally, retrieval confidence criteria should be considered. Averaged products are highly dependent on choices made for data aggregation and weighting, and sampling errors can be further propagated when deriving regional or global "mean" AOD. Different choices for aggregation and weighting result in estimates of regional and global means varying by 30% or more. The impacts of a particular averaging algorithm vary by region and surface type and can be shown to represent different tolerance for clouds and retrieval confidence.**

*Index Terms*—**Aerosol optical depth (AOD), averaging, global, Moderate Resolution Imaging Spectroradiometer (MODIS), monthly, sampling.**

## I. INTRODUCTION

**A**EROSOLS affect the climate system, but unlike greenhouse gases, their distribution, microphysical properties, and, thus, impact vary widely across multiple spatial and temporal scales. Depending on atmospheric conditions, aerosols can be transported over long distances from their sources as discrete plumes, can dissipate by mixing processes within the atmosphere, or may be quickly redeposited on the surface as a result of gravitational settling, cloud processing, or dry deposition. Because aerosol properties exhibit such large gradients on so many scales, no set of measurements can satisfy all scales necessary for understanding the true aerosol effect on climate. Some climate problems, however, can be studied using monthly statistics of aerosol properties [1].

Aerosol optical depth (AOD) is a first-order quantity in the Earth's radiative budget and is determined by certain properties (loading, size distribution, and refractive index) of the columnar aerosol. Aerosol direct radiative effect (DRE) is generally linearly correlated with AOD; thus, characterizing global AOD is a useful first step [2]. In cloud-free daylight conditions, AOD can be retrieved from passive satellite observations of solar reflectance. Given the low expected uncertainty of modern satellite retrievals [3], [4], it is tempting to use these products for addressing questions of aerosol trends, radiative forcing, and aerosol/cloud interactions. In fact, multiyear satellite data are being compared with each other and to models [5] to assess AOD trends [6] and to calculate climate effects [7].

Nominal satellite AOD products characterize the state of the atmosphere in the satellite's field of view (FOV) at overpass, so that a month's data essentially represent a composite of many overpasses. In hopes of making the data processing and interpretation less cumbersome for end users, satellite data teams may provide monthly statistics [8] of their own product. In addition, new Web-based analysis tools, such as Giovanni (http://giovanni.gsfc.nasa.gov/) [9], enable a user to easily visualize and analyze monthly AOD products. Although such tools and products enable a wide range of users to analyze satellite data, they should be used with caution.

Quantitative analyses of monthly satellite data products require a good understanding of the uncertainties of the FOV aerosol retrieval algorithm, as well as the temporal and spatial sampling of the products. The uncertainty in the retrieval algorithm is often assessed by comparing nominal satellite products to ground-truth observations, such as those from sun photometers [3]. For the purpose of this study, we will assume that, as a result of such "validation" exercises, satellite FOV data are unbiased during the overpass of the ground sites. The ground sites, however, have their own uncertainties and are unevenly distributed globally and temporally. This means that the ground-truth sun photometer data cannot provide an independent measure of the satellite sampling, in the way that radar measurements might provide for satellite estimates of rainfall [10].

Thus, present monthly aerosol statistics are created on incomplete sampling of a spatially and temporally inhomogeneous field. Since AOD values are derived only within the clear-sky satellite FOV, they will not represent AOD over nonobserved locations (e.g., overcast) and times of day (e.g., nighttime). In addition, since many of the sensors are in polar orbit, their sampling patterns exacerbate the problem. Each day, there are coverage gaps in the tropics, as well as multiple views of the summertime poles. Therefore, the orbital geometry, combined with avoidance of clouds and nighttime, leads to non-uniform and incomplete aerosol sampling. Furthermore, as each

sensor has its own sampling patterns and retrieval algorithms, comparison of AOD statistics becomes even more difficult.

Without an independent set of high-resolution and temporally continuous global aerosol measurements, a particular sensor's sampling errors are impossible to characterize definitively. Nonetheless, for other spatially varying fields, such as rainfall (comparing radar [10]) and wind speed [11], satellite sampling errors have been studied. These and other studies have suggested various methods for aggregating, weighting, and averaging spatially varying data, but none succeeds in resolving all the problems of integrating multiple temporal and spatial scales. Since aerosol properties and their retrieval algorithms are different than for either precipitation or wind speed, deriving monthly mean aerosol is a new and difficult challenge. Certain aerosol sampling biases are being studied, including assessment of subpixel cloud biases within fine- versus coarse-resolution data [12], [13] and bias adjustment for measurements at different times of day [14]. The fusion of model predictions through data assimilation techniques is also helping in understanding sample biases in aerosol properties and climate effects [15], [16], as well as detailed analyses of retrieval algorithm effects for representative case studies [17]. Nonetheless, there is still a great need to address issues of sampling in aerosol data, specifically those inherent in individual data sets.

Thus, we believe that any derivation of AOD statistics from existing satellite data suffers from sampling biases. Certain aggregations of the data enhance the clear-sky bias that is inherently present in nominal satellite retrievals, whereas others enhance aerosol signals from certain regions and aerosol conditions. Although we cannot identify a "best" way to derive monthly AOD statistics for all locations and aerosol conditions, derived from any sensor, in this paper, we show how different choices lead to different results.

We use a particular data set, specifically one year of data (2003) from the Moderate Resolution Imaging Spectroradiometer (MODIS) aboard the Terra satellite. We describe how the orbital (FOV) data are operationally aggregated and averaged to yield gridded daily means and then are pixel weighted to derive standard gridded monthly mean products. We demonstrate how confidence assessments can be used to derive alternative daily and monthly gridded data. For simplicity, we assume that each retrieved FOV aerosol value is sufficiently accurate and unbiased and represents the daily mean [18] at that location. We can therefore limit our study to data aggregation, weighting, and averaging. Nonetheless, we show that different choices for aggregating and weighting lead to divergent estimates of global monthly mean AOD. Particular averaging paths accentuate certain aspects of the global AOD distribution and therefore require different physical interpretation. While no averaging path truly captures all aspects of the sampling uncertainty of the global mean AOD, we might consider results from a range of approaches as a relative measure of uncertainty.

## II. MODIS ORBITAL DATA: L2

MODIS is a 36-channel spectrometer (0.412–14.2 $\mu$m) that views a 2300-km swath from aboard NASA's Terra and Aqua satellites at an altitude of 700 km. Each MODIS provides near-global coverage on 14–15 orbits per day. However, because MODIS is in polar orbit, there are gaps near the equator and multiple viewings of the poles. Near swath edges, view angles exceed $55°$, such that individual pixels can represent three times the surface area of nadir views.

The current (Collection 5 or C005) MODIS dark-target aerosol retrieval algorithms [19], [20] derive aerosol properties over dark land [21] and ocean [3], [22] within MODIS' FOV. Regardless of surface target, the algorithm carries out the following: 1) aggregates pixel-level spectral reflectance observations (at 500 m for most channels) into $10 \times 10$ km retrieval regions; 2) discards pixels contaminated by clouds and other factors; 3) truncates the lowest and highest 25% of the reflectance histogram if the retrieval is over water and the lowest 20% and highest 50% if the retrieval is over land; and, finally, 4) compares the average of the remaining values to a lookup table to derive AOD and fine-mode aerosol fraction over water and the fine-"model" aerosol fraction over land. Each pixel is assumed to represent a statistical sample of the spectral reflectance over the $10 \times 10$ km region. During the retrieval process [19], a wide variety of "quality-assurance" (QA) flags [23] are set, diagnosing any irregularities encountered during the retrieval process. Certain QA flags indicate less than optimal reflectance statistics, lack of clear sky, large standard deviation, or poor match with assumed lookup tables. At the retrieval's conclusion, a single flag is assigned as a summary. This is known as the "quality confidence" (QC) and is intended to represent the expected confidence of that particular retrieval. QC ranges from 3 (high) to 0 (low). A high QC value indicates that the algorithm performed under optimal conditions, it does not necessarily mean that the algorithm provided the "correct" solution. Nonetheless, one should expect the result to have less uncertainty under higher QC.

The combination of aerosol products and QA information (including QC), derived in the FOV along orbit tracks, is known as Level 2 (L2), grouped as files known as MOD04 (specifically MOD04_L2 for Terra and MYD04_L2 for Aqua). Each derived parameter is known as a scientific data set (SDS). Over ocean, the retrieved AOD and QA SDSs are as follows:

1) Effective_Optical_Depth_Average_Ocean;
2) Quality_Assurance_Ocean.

Over land, they are as follows:

1) Corrected_Optical_Depth_Land;
2) Quality_Assurance_Land.

The qualifiers Effective, Corrected, and Average relate to the AOD SDS' processing heritage [19] and do not have quantitative meaning here. Although both AOD SDSs represent multiple wavelengths, here, we consider only the reported values in the mid-visible (0.55 $\mu$m). For the QA SDSs, we consider only the summary QC flag. The joint AOD product, denoted as the Optical_Depth_Land_And_Ocean SDS, combines the two separate AOD products into one. In order to create a more "scientifically" useful product, graduation to the joint product is limited to higher confidence data (QC $\geq 1$) over land. Currently, there is no QC restriction over ocean. Taking into account the orbital geometry, and after eliminating bright (e.g., glint, deserts, and snow) and completely overcast targets,

retrieved high-confidence AOD data represent less than 10% of the globe each day.

MODIS AOD products have been validated by comparing with ground-truth sun-photometer measurements, usually obtained from the quality-controlled Aerosol Robotic Network (AERONET) [24]. Here, "validated" means that, in the cases where both MODIS and sun photometer provide high-confidence data, two-thirds of the ordered pairs (one standard deviation) match within some expected uncertainty. Although the C005 products have not yet been extensively validated, it is expected that sufficiently high confidence mid-visible AOD from MODIS will match within $\pm 0.03 \pm 5\%$ over ocean (QC $\geq 1$; [20]), and $\pm 0.05 \pm 20\%$ over land (QC $= 3$; [21]). Although the published fits are not exactly one-to-one, we will assume that MODIS provides an unbiased estimate of the "true" AOD, with lower uncertainty being associated with higher confidence.

## III. DAILY GRIDDED AOD (D3 PRODUCTS)

Chemical transport and general circulation models compute fields on grids at regular temporal and spatial resolutions. They are designed to provide continuous data that do not have "holes" or inconsistent sampling. Even when limited to 10% coverage of the globe daily, MODIS data are attractive for comparison with models [5], [7] and assimilation [15].

MODIS L2 data, however, while nominally $10 \times 10$ km, are not derived on a regular grid. Some pixels represent larger surface area than others, and the same orbit is repeated only every 16 days. Also, processing one day of L2 means stitching together approximately 135 segments (*granules*) that use nearly 1 GB of file space. One way to make the data manipulation easier for users is to provide statistics of the L2 data on a regular grid. These statistics (including mean, standard deviation, and histograms) are known as Level 3 products (or L3) [8] and, in the case of MODIS, are provided at $1° \times 1°$ resolution daily (L3-Daily or D3). In addition to providing useful spatial and/or temporal summaries, L3 data enable meaningful visualization (i.e., maps) of AOD distributions.

### A. Equal-Weighted (Simple) Mean

To understand the standard D3 products (MOD08_D3 for Terra and MYD08_D3 for Aqua files), we assume that each retrieved 10-km L2 AOD value is as follows: 1) measured independently; 2) unbiased; and 3) representative of the daily mean at that location [18]. Let us further assume that the assigned QC value is inversely related to retrieval uncertainty. For a collection of L2 values ($\tau_{\nu,j,l}$) in grid cell $l$ and day $j$, the generic daily mean ($\bar{\tau}_{j,l}$) is

$$\bar{\tau}_{j,l} = \sum_i W_{i,j,l}\tau_{i,j,l} \Big/ \sum_i W_{i,j,l} \qquad (1)$$

where $W_{i,j,l}$ is a weighting assigned to each L2 value. If each measurement is weighted equally, regardless of sampling or quality, then $W_{i,j,l} = 1$, and (1) represents the simple mean

($\bar{\tau}_{j,l}^{\text{Mean}}$). The simple mean of the L2 AOD SDS's (ocean, land and combined), are reported in D3 as the respective SDS's:
1) Effective_Optical_Depth_Average_Ocean_Mean;
2) Corrected_Optical_Depth_Land_Mean;
3) Optical_Depth_Land_And_Ocean_Mean.

The qualifier Mean that is appended to the L2 SDS name refers to this particular aggregation (simple mean) from L2 to D3. The numbers of L2 pixels represented by each grid cell are known as pixel counts (PC or $P_{j,l}$) and are reported in D3 as SDSs with the appended qualifier Pixel_Counts. Generally, PC ranges from 0 to 120 and depends on season, latitude, and local conditions. Additional L2 statistics (e.g., standard deviation, max, min, etc.) are also included in D3 but are not discussed further in this paper. Note that the joint land-and-ocean Mean product represents the L2 data that have already been QC filtered (QC $\geq 1$ over land). Compared to $< 10\%$ daily coverage of the L2 individual 10-km-resolution retrieval regions, the D3 data effectively increase global coverage (of $1° \times 1°$ boxes) to $\sim 30\%$ per day, depending on the season.

Whether a particular $1° \times 1°$ value represents a "true" daily mean AOD depends on the L2 sampling compared to true AOD spatial and temporal variability. Anderson *et al.* [2] suggest that the spatial scale of aerosol coherence is somewhere between 40 and 200 km, depending on the situation. The degree of correlation between AOD data on $0.5°$ ($50 \times 50$ km) and point measurements provides the basis for many satellite AOD product validations [25], including those for MODIS. Where AOD gradients are small (far from clouds and sources), the average over a $1°$ box should be statistically sufficient for calculating the representative mean for that box. On the other hand, where AOD gradients are large or the sampling in the box is too small, the simple averages may not be representative. One should note that the D3 processing does not eliminate the pathological case of a single L2 pixel ($10 \times 10$ km) representing an entire $1° \times 1°$ box.

### B. Confidence-Weighted Mean

Since we expect lower uncertainty for higher confidence data, we might consider weighting the average toward higher confidence data. This daily *confidence-weighted* mean QA_Mean AOD product (sometimes called quality weighted) is

$$\bar{\tau}_{j,l}^{\text{QA\_Mean}} = \sum_i Q_{i,j,l}\tau_{i,j,l} \Big/ \sum_i Q_{i,j,l} \qquad (2)$$

where the weights are set to the L2 QC values ($W_{i,j,l} = Q_{i,j,l}$). Thus, the lowest confidence data (QC $= 0$) receive zero weight. The daily *total confidence* ($Q_{j,l}$) for a given grid cell is the sum of the QC-value histogram ($Q_{j,l} = \sum_i Q_{i,j,l}$) and has a maximum possible value of about 360 (i.e., $120 \times 3$). In D3, there are two QA_Mean products that are as follows:
1) Effective_Optical_Depth_Average_Ocean_QA_Mean;
2) Corrected_Optical_Depth_Land_QA_Mean.

The QC-value histogram associated with each $1° \times 1°$ cell is also retained in D3. Note that there is no corresponding QA_Mean for the joint product (which is not QA weighted).

Compared to the Mean product, the filtered QA_Mean product reduces global coverage by 1% or less. Differences between the D3 Mean and D3 QA_Mean AOD values are generally small ($|\Delta \tau| < 0.01$) but systematic. Over land, a higher AOD is often associated with brighter scenes (e.g., near dust aerosol sources). Because of brighter surfaces, higher AOD values for these scenes will have lower QC, resulting in QA_Mean < Mean. Over ocean, a very low AOD (small aerosol retrieval signal-to-noise ratios) is often associated with larger retrieval fitting errors, resulting in lower QC for low AOD values. Thus, the low AOD pixels get less weight, leading to QA_Mean > Mean. This is especially common over the Southern Hemisphere (SH), where AOD is commonly low.

Currently, the Giovanni Web tool allows for analysis of the joint Mean SDS (Optical_Depth_Land_And_Ocean_Mean) only but provides the ability to average over each surface separately. Because the joint product only includes higher confidence data, its interpretation should be different than that if using the separate ocean and land (QA_Mean or Mean) products. Except for the most basic exploratory analysis, we suggest using the separate products rather than the joint.

## IV. MONTHLY GRIDDED AOD (INCLUDING M3 PRODUCTS)

For climate applications, such as computing aerosol DRE [1], monthly averaged data would be more convenient than the daily aggregates. They have fewer holes than the daily data, and are far less computationally expensive to process, globally. The question is how to compute monthly data. Gridded monthly products can be derived either from the original L2 or from the D3 aggregates of the L2. If we believe that the D3 SDS (e.g., Mean, QA_Mean, PC and QC-value histograms) capture sufficient statistics of the L2, then we prefer to use the D3 because they are much less computationally demanding.

Starting from D3, the generic monthly mean AOD ($\overline{\overline{\tau}}_{k,l}$) for month $k$ and grid cell $l$ is

$$\overline{\overline{\tau}}_{k,l} = \sum_j X_{j,l} \bar{\tau}_{j,l} \Big/ \sum_j X_{j,l} \qquad (3)$$

where $X_{j,l}$ is the weighting chosen for the day $j$ and location $l$ and $\bar{\tau}_{j,l}$ may be either the Mean or the QA_Mean D3 product. When assigning weights, we need to decide whether each day's D3 value should have equal weighting or should reflect L2 sampling in some way. For this section, we will assume that, no matter the sampling of L2, each day's D3 product is a good representation of the "true" daily mean. As long as there are minimal day-to-day changes in the AOD and each day's retrieval has high confidence, only a few days may be needed to represent the monthly mean. This means that *equal day weighting* (i.e., $X_{j,l} = 1$) would be appropriate. For conditions of low cloud fraction and regularly occurring aerosol plumes (e.g., Saharan dust over ocean during springtime), if the relative maxima and minima are sampled proportionally to their occurrence, equal day weighting may also be appropriate. Fig. 1(a) shows a gridded map of the number of daily AOD values used in computing a monthly mean (May 2003) from the

D3 data (Terra). Fig. 1(b) shows the equal-day-weighted mean derived from the D3 Mean ($\overline{\tau_{k,l}^{\mathrm{Day,Mean}}}$). Although the over-land and over-ocean data are treated separately, they are presented as combined plots in the figure. Typical known springtime aerosol features (e.g., Saharan dust transport and east Asian dust/pollution plume) are clearly evident. From the ~30% global coverage of D3 Mean during each day of May 2003, the monthly product increases $1° \times 1°$ grid coverage to nearly 70%. Presumably, the remaining 30% of the globe is avoided due to polar night, snow cover, bright surface, or persistent cloudiness.

### A. Threshold Equal Day Weighting

In the path of a midlatitude storm (having complex cloud and aerosol features), one particular day may be represented only by a single L2 value. Unless we used a mean value pixel, or the AOD has minimal spatial gradients each day, the D3 value will be biased. However, we might expect that a day with a hundred L2 pixels will enable a better estimate of the mean. Instead of biasing our result to poorly sampled days, we may include only days having at least some minimal sampling. Here, we introduce the *threshold equal day weighting*, where we assign a minimum sample of L2 pixels ($P_{j,l} > t$) for that day's AOD information to be included in the grid location's monthly mean, e.g.,

$$\overline{\tau_{k,l}^{\mathrm{Day}Pt}} = \sum_{j(P_{j,l}>t)} \bar{\tau}_{j,l} \Big/ \sum_{j(P_{j,l}>t)} 1. \qquad (4)$$

The results are sensitive to the chosen value of $t$. As we increase $t$, we tend to reduce not only the "anomalous" of very high (and likely unrealistic) values of monthly mean AOD but also global coverage. We find that setting the threshold to 5 (i.e., $P_{j,l} > 5$) visually balances minimal anomalous features and hole-free monthly maps, reducing global coverage by only 2% compared to the nonthreshold approach. Fig. 1(c) shows the number of days meeting the PC threshold ("Day5"), whereas Fig. 1(d) is the difference between the "Day5" monthly mean and that shown as Fig. 1(b) (e.g., $\overline{\tau_{k,l}^{\mathrm{DayP5,Mean}}} - \overline{\tau_{k,l}^{\mathrm{Day,Mean}}}$). Specifically over cloudy storm tracks (in both hemispheres), the PC threshold reduces the number of days included in the aggregation. The resulting AOD map shows some increases and some decreases, but generally, $\overline{\tau_{k,l}^{\mathrm{DayP5,Mean}}} \le \overline{\tau_{k,l}^{\mathrm{Day,Mean}}}$ over both land and ocean for most of the globe. Because poorly sampled days are often due to extensive cloudiness, threshold equal day weighting tends to eliminate cloud contamination. In other words, the application of the threshold will bias the result toward the clear-sky AOD that generally has a lower magnitude. However, since cloudiness is not the only reason for low sampling (also orbital gaps, snow, glint, and bright surfaces), differences at every location must be interpreted separately.

### B. Pixel Weighting

Another way to reduce the impact of poorly sampled days, but without reducing global coverage, is by applying *pixel*
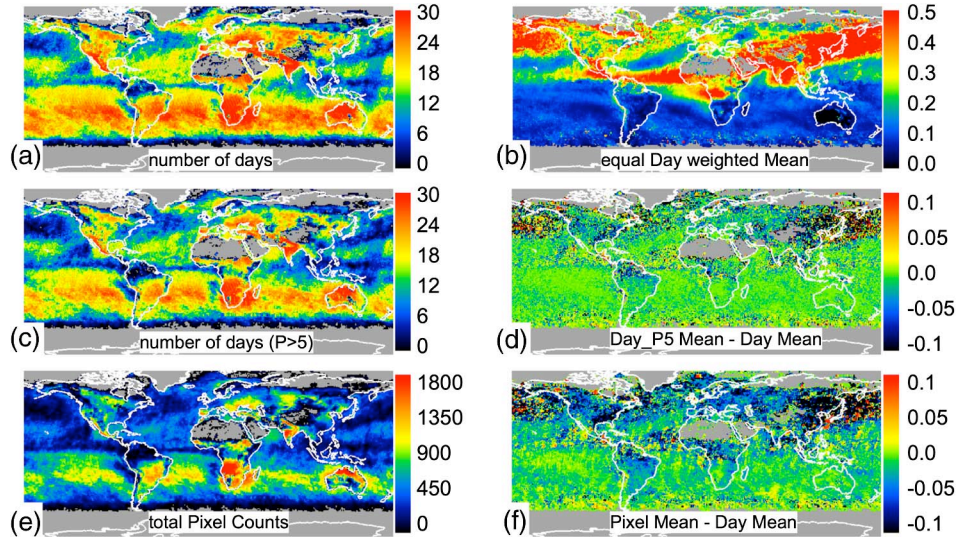
Fig. 1.   May 2003 monthly mean dark-target AOD on $1° \times 1°$ grid, calculated from equal-day- and pixel-weighted D3 Mean data. Separate land and ocean products are combined on each map. (a) Number of days with valid data. (b) Monthly mean computed from equal day weighting. (c) Number of days where $P_{j,l} > 5$. (d) Difference between means computed from pixel ($P_{j,l} > 5$) and equal day weightings. (e) Total monthly PCs. (f) Difference between means computed from pixel and equal day weightings. Note the different color scales to the right of each panel.

*weighting*, such that we weight each day's contribution by its PC, i.e.,

$$\overline{\overline{\tau_{k,l}^{\text{Pixel}}}} = \sum_j P_{j,l}\bar{\tau}_{j,l} \bigg/ \sum_j P_{j,l} \qquad (5)$$

where $P_{j,l}$ is the daily PC for day $j$ and location $l$. Days with a hundred L2 measurements are weighted a hundred times more than days with a single measurement. Fig. 1(e) shows the monthly total gridded PC (i.e., $P_{k,l} = \sum_j P_{j,l}$) for May 2003. Not surprisingly, monthly PC distribution is generally correlated with the number of days for which there are valid observations [Fig. 1(a)]. However, for some regions, (e.g., North America), a larger number of days does not necessarily relate to higher PC. This area may be characterized with cloud fields that are on the order of 10 km (reducing daily PC), which are not covering the entire $1° \times 1°$ box. Fig. 1(f) shows the differences between the pixel- and equal-day-weighted means, both derived from the D3 Mean (e.g., $\overline{\overline{\tau_{k,l}^{\text{Pixel,Mean}}}} - \overline{\overline{\tau_{k,l}^{\text{Day,Mean}}}}$). Similar to the application of a daily threshold, pixel weighting tends to derive lower AOD values over much of the globe (both land and ocean). Yet, pixel weighting does not reduce global coverage, as does the threshold screening.

An interesting property of the pixel-weighted monthly mean derived from the D3 Mean is that it exactly preserves the sampling of the L2 data for the month. In other words, combining (1) and (4), it is easy to show that the pixel-weighted D3 Mean is equivalent to simple averaging of the L2, i.e.,

$$\overline{\overline{\tau_{k,l}^{\text{Pixel,Mean}}}} = \sum_j P_{j,l}\bar{\tau}_{j,l}^{\text{Mean}} \bigg/ \sum_j P_{j,l} = \sum_{i,j} \tau_{i,j,l} \bigg/ \sum_{i,j} 1. \quad (6)$$

The pixel-weighted mean represents the sampling pattern of a given sensor, and different sensors will provide different estimates of a location's monthly mean. All may be biased esti-

mates of the "true" monthly AOD. As with the pixel-threshold equal-day-weighted mean (described in Section IV-A), the pixel-weighted mean reduces the impact of cloud and bright surface contamination. Thus, it is also clear sky and darker target biased, which, in general, avoids the larger values (anomalous) of AOD. Although pixel weighting tends to provide reduced AOD over much of the globe compared to equal day weighting, there are regions where the opposite is true.

### C. Threshold Pixel Weighting

To ensure even less contamination from clouds and bright surfaces, one may choose to combine both pixel weighting (Pixel) and daily PC (P5) thresholds for computing a monthly aggregate. Generally, the threshold value of $t = 5$ ($P_{j,l} > 5$) will remove poorly sampled days without sacrificing global distribution and without noticeably reducing the number of L2 pixels available for the aggregate [e.g., Fig. 2(a)]. We can use (4) and (5) to derive the PixelP5-weighted monthly mean from the D3 Mean, $\left(\overline{\overline{\tau_{k,l}^{\text{PixelP5,Mean}}}}\right)$, i.e.,

$$\overline{\overline{\tau_{k,l}^{\text{PixelP5,Mean}}}} = \sum_{j(P_{j,l}>5)} P_{j,l}\bar{\tau}_{j,l}^{\text{Mean}} \bigg/ \sum_{j(P_{j,l}>5)} P_{j,l}. \quad (7)$$

In fact, the operational monthly aggregation algorithm computes this quantity, which is called the Mean_Mean product. In the standard gridded monthly MOD08_M3 (or M3) files [8], the Mean_Mean AOD products include the following:

1) Effective_Optical_Depth_Average_Ocean_Mean_Mean;
2) Corrected_Optical_Depth_Land_Mean_Mean;
3) Optical_Depth_Land_And_Ocean_Mean_Mean.

Fig. 2(b) shows May 2003's PixelP5-weighted Mean monthly product (the M3 Mean_Mean product), computed over ocean and land separately and combined as one image. Compared to our gridded equal-day-weighted mean [Fig. 1(b)],
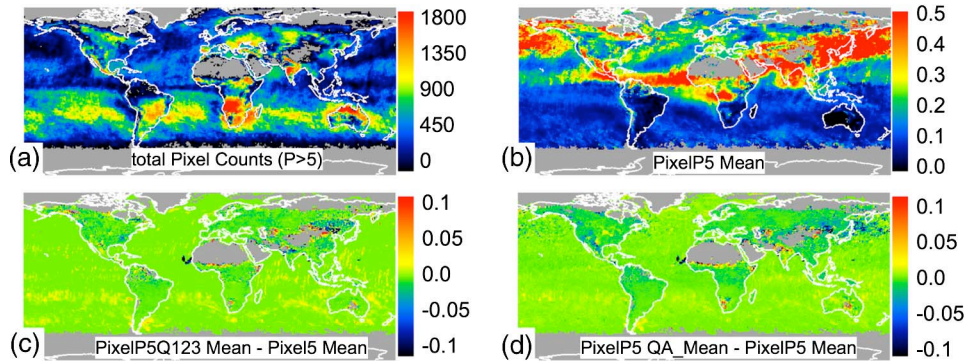
Fig. 2. May 2003 monthly mean dark-target AOD on $1° \times 1°$ grid, calculated from pixel-weighted D3 Mean and QA_Mean data. Separate land and ocean products are combined on each map. (a) Total monthly PCs summed for days where $P_{j,l} > 5$. (b) Monthly mean computed from pixel weighting of the Mean for the days with $P_{j,l} > 5$. (c) Difference if counting pixels that meet both PC and QC thresholds ($P_{j,l} > 5$ and $Q_{i,j,l} \geq 1$). (d) Difference if pixel weighting is applied to the QA_Mean instead of the Mean. Note the different color scales to the right of each panel. Also note that panel A is equivalent to the M3 Mean_Mean product.

some of the extremely high values over NH midlatitude storm belts have been reduced, whereas the main features of the global aerosol distribution remain intact. Except for a few grid boxes that have all days screened by the daily PC threshold, most PixelP5 values will be very similar to straight Pixel Mean values (not plotted).

Instead of only a PC threshold, we might consider a QC threshold for screening low-confidence data. Although the joint product (Optical_Depth_Land_And_Ocean) is QC screened in L2 ($Q_{i,j,l} \geq 1$ over land), it does not retain the QC information in D3. Since the separate over-land and over-ocean D3 products retain the QC-value histogram, one can use QC to exclude lower confidence days from the monthly aggregate. Thus, the separate products allow for more freedom in their analysis. For example, $\overline{\overline{\tau_{k,l}^{\mathrm{PixelP5Q123,Mean}}}}$ represents the monthly mean, computed by pixel weighting only days having more than five pixels and at least marginal confidence ($Q_{i,j,l} \geq 1$), i.e.,

$$\overline{\overline{\tau_{k,l}^{\mathrm{PixelP5Q123,Mean}}}}$$
$$= \sum_{j(P_{j,l} \geq 5)} P_{j,l}^{(Q_{i,j,l} \geq 1)} \bar{\tau}_{j,l}^{\mathrm{Mean}} \bigg/ \sum_{j(P_{j,l} \geq 5)} P_{j,l}^{(Q_{i,j,l} \geq 1)} \quad (8)$$

where $P_{j,l}^{(Q_{i,j,k} \geq 1)}$ represents the number of pixels having $Q_{i,j,l} \geq 1$. In effect, we have reduced the pixel weighting of lower quality D3 data. Fig. 2(c) shows the differences between this PixelP5Q123 and the PixelP5 (M3 Mean_Mean) products shown in Fig. 2(b). Over ocean, the largest differences can be seen in the clean SH. Since both AOD and QC are lower there, removing some of the very lowest AOD values tends to increase the mean. Over land, the differences are generally small but tend to be slightly negative. Differences are largest over brighter surfaces (e.g., North America, eastern Asia), where retrievals are likely to have lower confidence. Applying both the QC and PC thresholds to pixel weight, the over-land SDS produces results similar to those for which only the PC threshold is applied, but the process is not exactly equivalent to pixel weighting the over-land portion of the combined product. Applying both QA and PC thresholds further decreases global coverage by 1%. Over land, there are few QC values of 1 or 2, so changing the threshold to QC $\geq 2$ provides little additional screening.

## D. Confidence Weighting

Operational M3 processing uses threshold $(P > 5)$ pixel weighting to aggregate PCs [e.g., Fig. 2(a)] and to derive monthly products from the D3 QA_Mean product. This aggregation $(\overline{\overline{\tau_{k,l}^{\mathrm{PixelP5,QA\_Mean}}}})$ is only derived from the separate land and ocean SDSs. In the standard M3 products, these parameters are known as the QA_Mean_Mean. Fig. 2(d) shows the differences between the PixelP5-weighted D3 QA_Mean (equivalent to the M3 QA_Mean_Mean) and the PixelP5-weighted D3 Mean (equivalent to the M3 Mean_Mean). Over land, QA_Mean_Mean < Mean_Mean, primarily due to lower confidence over brighter and cloudier targets. Over ocean, differences are generally small but are slightly positive (yellow patches) in some regions.

This means that L2 measurement quality is used as a weight when calculating the D3 QA_Mean product; however, day-to-day quality differences are not assessed when forming the standard M3 QA_Mean_Mean product. For example, consider a pathological case of one day having 100 pixels, where one pixel has QC = 3, and the rest have QC = 0. Although the D3 QA_Mean represents the sole high QC pixel, the M3 QA_Mean_Mean would weight this day as 100 pixels. The QA_Mean_Mean does not preserve the L2 confidence information, and thus, it can inconsistently weight days with high PC but zero (or low) confidence.

Starting with the D3 QA_Mean product, and setting daily weights to the total confidence [e.g., $X_{j,l} = Q_{j,l}$ in (3)] we can derive the *confidence-weighted* monthly mean $(\overline{\tau_{k,l}^{\mathrm{Conf,QA\_Mean}}})$. If no pixel or QA thresholds are applied, this formulation preserves the confidence sampling of the L2. Fig. 3(b) shows the total monthly confidence ($Q_{k,l} = \sum_j Q_{j,l}$) for May 2003, over dark land and ocean separately, combined as one map. One can see how the distribution of total confidence is not triple the PCs. Fig. 3(c) shows how this new confidence-weighted monthly mean differs from that produced as the standard M3 QA_Mean_Mean product [Fig. 3(a)]. Over ocean, the confidence-weighted AOD tends to be larger by 0.02–0.05, even over the SH where the AOD is low to begin with. We believe that the monthly confidence weighting magnifies the confidence weighting of the D3 QA_Mean (Section III), accentuating situations with strong aerosol signal. Over land, most
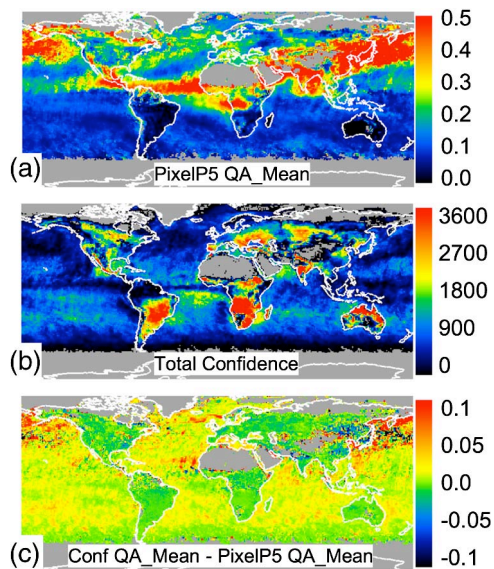
Fig. 3. May 2003 monthly mean dark-target AOD on $1° \times 1°$ grid, calculated from pixel- and confidence-weighted D3 QA_Mean data. Separate land and ocean products are combined on each map. (a) Monthly mean computed from pixel weighting of the QA_Mean for the days with $P_{j,l} > 5$. (b) Total monthly confidence. (c) Difference if confidence weighting is applied to the QA_Mean instead of pixel weighting (days with $P_{j,l} > 5$). Note the different color scales to the right of each panel. Also note that panel A is equivalent to the M3 QA_Mean_Mean product.

differences are smaller and nearly always negative. Due to the structure of the QA assessment, there are very few L2 pixels with QC = 1 or QC = 2, so that the number of QC = 0 is similar to QC = 3. Thus, differences between our new confidence-weighted mean and the standard M3 QA_Mean_Mean are small. Over both land and ocean, some aerosol hotspots (e.g., African dust and Asian dust/pollution plumes) show large positive differences, although the Asian plume is marked by both large increases and large decreases. Presumably, as the Asian plume is entrained within midlatitude weather systems, optically thick and inhomogeneous aerosol could be confused with clouds.

## V. MONTHLY GLOBAL MEAN AOD

In Section III, we explained how MODIS data are aggregated from L2 to D3. In Section IV, we showed how different choices for aggregating and weighting D3 lead to standard M3, as well as alternative monthly gridded products. At each step, we essentially asked whether the data to be aggregated should be considered equally representative of some "truth" or whether we need to apply selection (PC or QC thresholds) or weighting (e.g., pixel or confidence) schemes. We also considered whether this information should be propagated to subsequent aggregations. Equal weighting (whether from L2 to D3, or D3 and on) assumes that each data value is equally representative of the "true" mean value. Pixel weighting biases the result towards regions or days with larger L2 data sampling, whereas confidence weighting biases the result towards regions or days with higher L2 confidence. Thresholds may be added to completely remove regions or days with poor sampling or confidence. Although

each aggregation method provides a different solution, all tend to introduce clear-sky biases.

These considerations can be taken to the next step, i.e., computation of monthly global mean AOD. Regardless of whether it makes real physical sense to do so, climate models tend to lean on satellite data to provide guidance (e.g., [1]). How do different choices for aggregation, weighting, and averaging propagate when deriving the *monthly global mean* AOD $(\overline{\overline{\tau_k}})$? Let us begin with our D3 products (Mean, QA_Mean, PC, and QC-value histogram).

### A. Monthly Global L2 Sampling and Confidence

Before considering the computation of monthly global mean AOD, we shall consider the monthly global L2 sampling (total PC) and confidence (total Q). Although oceans dominate the surface area of the globe, the stricter requirements for over-ocean retrieval (avoidance of glint, coastlines, and ice) are such that the number of attempted L2 retrievals ($1.1 \times 10^8$ per month) is surprisingly similar to that attempted over land. Including multiply sampled data (the summertime pole), valid AOD values are retrieved for only about 6% and 12% of the pixels over land and ocean surfaces, respectively. High-confidence data (QC = 3) account for approximately 60% and 25% of the valid data over land and ocean, respectively, while at least marginal-confidence data (QC $\geq$ 1) account for about 85% and 98%, respectively. Although this may seem counter to the understanding that over-ocean AOD should be more accurate than over-land AOD, the seeming inconsistency reflects the algorithms' stricter criteria for high confidence over ocean. Weak aerosol signal over ocean (low AOD and extensive cloud decks) is common and flagged by low QC.

Fig. 4 shows the time series (Terra, 2003) of monthly total PC ($P_k = \sum_{i,j,l} P_{i,j,l}$) and total confidence ($Q_k = \sum_{i,j,l} Q_{i,j,l}$), as well as the PC distribution associated with each QC value. One can see strong maxima in both PC and confidence over land during the northern summer, with much less seasonal dependence over ocean. Interestingly, over ocean, the maximum in PC is not associated with the maximum in confidence. Note that because of different QA criteria, land is dominated by QC = 3, whereas the ocean is usually QC = 1.

### B. Ordering of Spatial and Temporal Averaging

To obtain a monthly global mean AOD, we are essentially performing *temporal* averaging over all days $j$ and *spatial* averaging over all grid cells $l$. These operations are not necessarily commutative, meaning that we must also consider their *order*. Consistent with Section IV, we will consider temporal averaging to be associated with weighting $X$ and assume that all measurements within a $1° \times 1°$ grid cell are random samples from the same population. Spatial averaging will be associated with weighting $Y$. We may first derive a monthly map, as in Section IV, and then take the average of the map, i.e.,

$$\overline{\overline{\tau_k}}^{j \text{ then } l} = \sum_l Y_l \left( \sum_j X_{j,l} \bar{\tau}_{j,l} \Big/ \sum_j X_{j,l} \right) \Big/ \sum_l Y_l \quad (9)$$
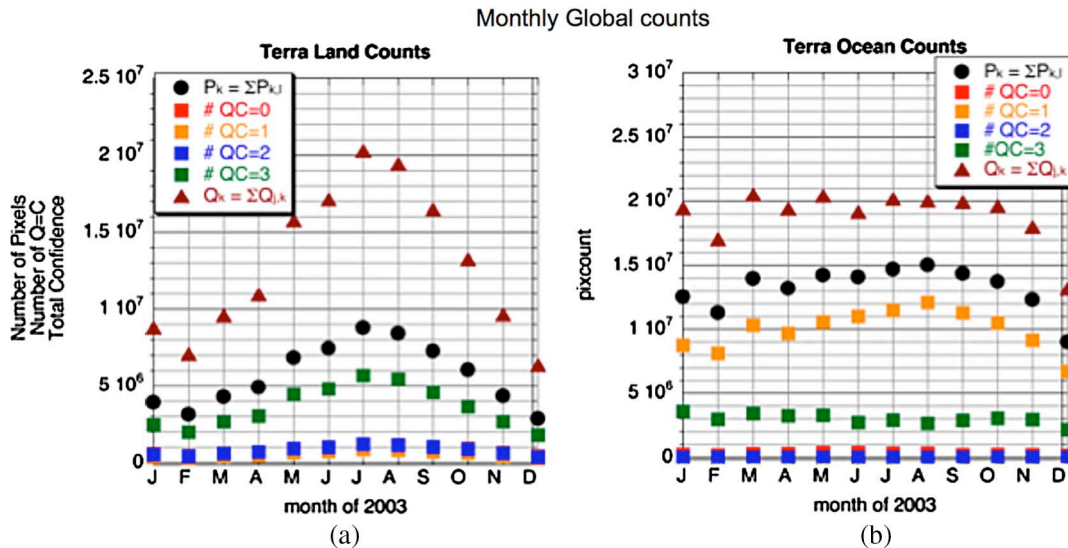
Fig. 4. Time series (Terra, 2003) of monthly total counts over (a) land and (b) ocean. For each panel, the black circles represent the monthly total PCs ($P_k$), the squares are the total PCs that are a given QC value, and the red triangles are the total confidence for that month (i.e., $Q_k = \sum_i Q_{i,k}$). Note the different seasonal dependences of the curves.

or we might reverse the order of averaging, such that

$$\bar{\bar{\bar{\tau}}}_k^{l \text{ then } j} = \sum_j X_j \left( \sum_l Y_{j,l} \bar{\tau}_{j,l} \middle/ \sum_l Y_{j,l} \right) \middle/ \sum_j X_j \quad (10)$$

where the first step creates daily global means and the second one derives the monthly mean. In either case, different weightings and thresholds can be applied at either or both steps. As before, only specific combinations preserve the L2 sampling and/or QA information.

For a noncommutative spatiotemporal average, each D3 cell's value is anchored to a particular day and grid-cell location. However, if each D3 cell is assumed to be spatially and temporally independent (anchoring forgotten), then we can derive the *straightforward* monthly average from all available D3 grid cells, i.e.,

$$\bar{\bar{\bar{\tau}}}_k^{\text{straight}} = \sum_{j,l} Z_{j,l} \bar{\tau}_{j,l} \middle/ \sum_{j,l} Z_{j,l} \quad (11)$$

where $Z_{j,l}$ represents the weighting given to a particular cell. One can show that setting $Z_{j,l} = P_{j,l}$ (pixel weighting, with no thresholds) exactly preserves the sampling of L2 during a month. Similarly, setting $Z_{j,l} = Q_{j,l}$ exactly preserves the L2 QA information. Setting $Z_{j,l} = 1$ presumes equal cell weighting (each grid/location is independent). Of course, since aerosol properties in neighboring L2 pixels are rarely independent, the straightforward average should not be expected to approximate global AOD. Nonetheless, this straightforward average is useful because it best approximates the sensor's sampling, in essence its "perception" of the global average.

Fig. 5 uses D3-like AOD data for four days and nine grid cells to illustrate how the choice of ordering can lead to divergent estimates of the global monthly mean AOD. On day 1, the AOD is homogeneous with low magnitude ($\tau = 0.1$, light blue). On days 2–4, an aerosol plume (with $\tau = 0.5$, red) passes from the top left to the bottom right of our domain. On day 3, the

middle cell is completely cloudy (no retrieval). The paths of "temporal then spatial" (9), "spatial then temporal" (10), and "straightforward" (11) are presented from left to right, top to bottom, and diagonal, respectively. Here, we used "equal cell weighting" (where all weights are 1). Along each path, the number of cells that were averaged is given in parentheses. The color of a grid cell approximately represents the AOD magnitude retrieved during that step. The result of our example case is that the final "global" AOD will range between 0.189 and 0.194, meaning that there is 2.7% difference due only to our choice of ordering. The ordering is noncommutative when there is missing sampling, and this fact is not reflected in weighting computation.

What if there exist gradients of sampling, as well as gradients of AOD? Fig. 6 assumes the same initial AOD distribution as Fig. 5 but includes L2 PC as information (in parentheses) within each grid cell. In our artificial case, generally, we see higher PC associated with lower AOD. For our first step, we apply pixel weighting in the first step and equal cell weighting in the second step. From left to right, the first step is analogous to operational M3 processing (temporal averaging with pixel weighting). The second step is equivalent to deriving a global average from the M3 map. The path from top to bottom represents spatial (with pixel weighting) then temporal averaging. The diagonal path is straightforward averaging (assuming pixel weighting only). Here, the global mean differences range by more than 16% (from 0.164 to 0.191). In this case, the pixel weighting results in a clear-sky bias toward lower AOD but not for all orderings.

As mentioned before, straightforward averaging is equivalent to ordered averaging with consistent application of weights. If there are no empty grid cells for any day (as in model or continuously interpolated data), or there are empty cells but all weights are computed and applied consistently, the ordering is commutative, and all paths yield the same result as straightforward averaging. However, if there are missing or

This article has been accepted for inclusion in a future issue of this journal. Content is final as presented, with the exception of pagination.

LEVY *et al.*: CRITICAL LOOK AT DERIVING MONTHLY AEROSOL OPTICAL DEPTH FROM SATELLITE DATA
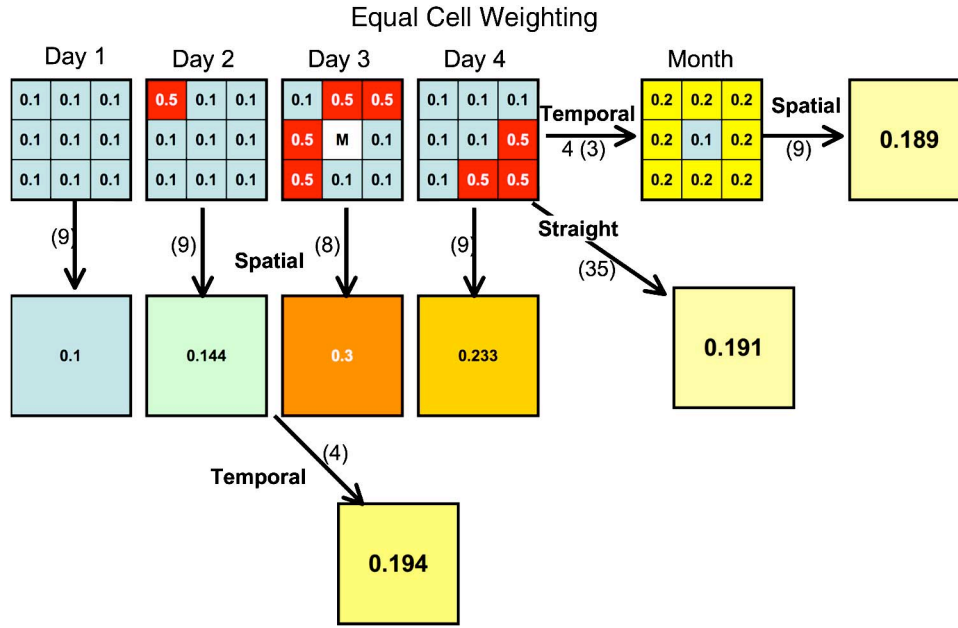
9

Fig. 5. Different paths to estimating the global monthly mean AOD from four days and nine grids of artificial AOD data. The AOD is homogenous with low magnitude ($\tau = 0.1$; light blue) on day 1. Days 2–4 show a plume ($\tau = 0.5$; red) moving from the top left to bottom right. On day 3, the middle cell has no value retrieved, presumably due to cloud. Paths from left to right, top to bottom, and diagonal represent the ""different ordering of "temporal then spatial," "spatial then temporal," or "straightforward" averages, respectively. All weighting is "equal cell." The number of grid cells used in the average is given in parentheses along the path. The color of a grid cell approximately represents its magnitude.
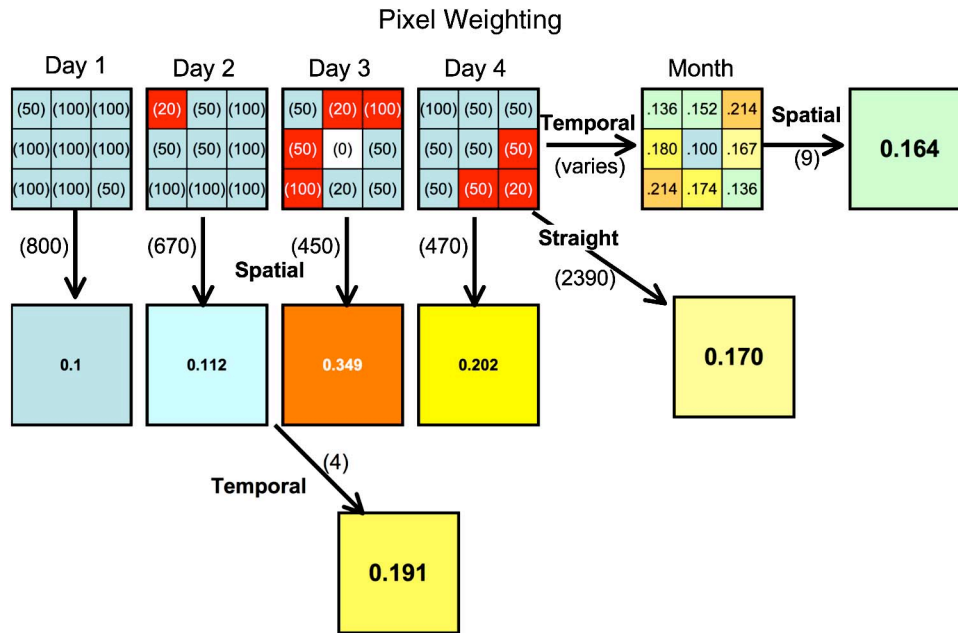


Fig. 6. Different paths to estimating the global monthly mean AOD from four days and nine grids of artificial AOD data, having the same magnitudes and distribution as for Fig. 5, but with the L2 PC presented (in parentheses) for each grid cell. Paths from left to right, top to bottom, and diagonal represent the different ordering of "temporal then spatial," "spatial then temporal," or "straightforward" averages, respectively. Pixel weighting (no thresholds) is applied for the first step, while equal cell weighting is used for the second step. The number of grid cells used in the average is given in parentheses along the path. The color of a grid cell approximately represents its magnitude.

sparse observations, and weights are not changed accordingly, the ordering will be noncommutative.

In addition to those choices detailed earlier, there are other valid choices for aggregation and weighting. We may apply thresholds (e.g., PC ≥ 5) or other weightings at any step along the way. We should also consider whether to weight each $1° \times 1°$ grid-cell location into the global average. Since Earth is a sphere, grid-cell surface area decreases toward the poles. "Latitude" weighting, or weighting a grid location by the cosine of latitude, is roughly equivalent to equal area weighting. Latitude weighting better represents a true global field (as in modeled or other uniformly gridded data) but may exaggerate latitudinal differences for a polar-orbiting instrument, where sampling is partially a function of latitude. In the next section,
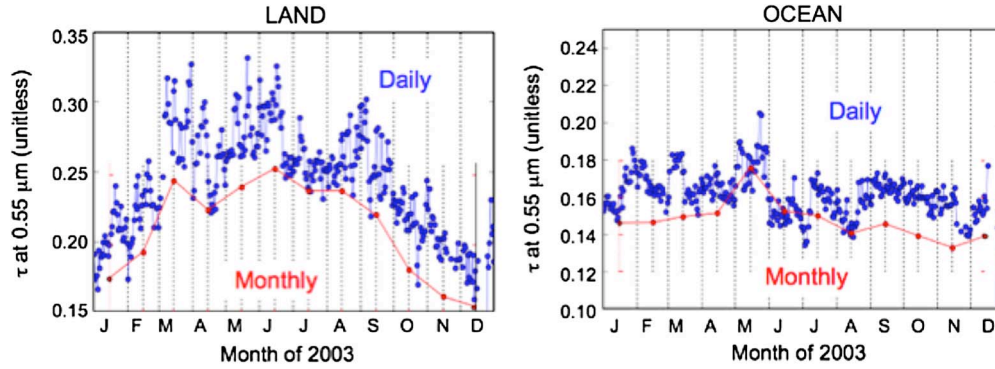
Fig. 7. Area-weighted global mean daily D3 (blue) and monthly M3 (red) AOD (over land and ocean separately) time series for 2003, obtained from the Giovanni Web site http://giovanni.gsfc.nasa.gov/. Note that the Giovanni tool utilizes only the D3 and M3 combined products (Optical_Depth_Land_And_Ocean_Mean and Optical_Depth_Land_And_Ocean_Mean_Mean) but provides the ability to average over each surface separately.

we apply some reasonable thresholds and tests toward deriving global averages of real MODIS data.

*C. Global AOD From MODIS*

Fig. 7 uses Giovanni-produced time series to demonstrate that the problem of noncommutative averaging order applies to MODIS data in particular. Giovanni easily creates global time series by computing equal area (latitude-weighted) averages from either monthly (M3) or daily (D3) aggregations of the combined AOD product. Shown in Fig. 7 are monthly (2003) time series from Terra, separated into over-dark-land (left) and over-ocean (right) surfaces. For each panel, blue points represent spatial averages of the MODIS standard D3 Mean product, whereas red points are spatial averages of the M3 Mean_Mean product. The M3 time series are systematically lower than the daily ones by about 10%, because this M3 product is a pixel-weighted product, whereas the D3 product is not. In general, the pixel weighting tends to bias the result toward lower AOD observations that represent clear-sky conditions. However, the bias varies by surface type and season, and it is beyond the scope of this paper to analyze the interplay of orbital geometry, bright surface avoidance, cloud cover, and true AOD. Although a casual user can easily compute global means from available data products, Fig. 7 shows why proper interpretation is necessary.

Table I presents the global monthly mean (for May 2003) computed from Terra-MODIS D3 Mean products over land and ocean separately. Presented are results from 28 different schemes for aggregation, ordering, and weighting. Choices include which D3 parameter to use (D3 Mean: #1–19 or D3 QA_Mean: #20–28), which ordering to apply (temporal then spatial: #1–8 and #20–24; spatial then temporal: #9–16 and #24–26; or straightforward: #17–19 and #27–28), and which weighting to use (equal cell/day, pixel and/or confidence, with or without thresholds, and latitude weighting). The last column lists aggregations of other MODIS products (e.g., L2 or M3) that derive equivalent results. For the choices presented here, global AOD over land ranges from 0.213 to 0.320 (50% difference), and that over ocean ranges from 0.153 to 0.222 (45% difference). The maximum values (shown in red font)

for both ocean and land are derived from temporal (equal day weighting) then spatial (equal cell weighting) averaging (#1). Minimum values (shown in blue) are derived from different schemes. Each choice of averaging order has a maximum value when weights are assumed equal at each step (#1, #9, #17, #20, #24, and #27). In comparison, lower mean AODs are derived when either threshold or pixel weighting is introduced. Confidence weighting leads to the lowest results over land, whereas pixel weighting leads to the lowest values over ocean.

Let us take a "base" result (#5: 0.257 for land and 0.184 for ocean; shown in bold font) to be the case that starts with the D3 Mean product; performing first temporal averaging using pixel weighting ($P > 5$ threshold) and then applying equal area weights for a spatial average. This is equivalent to equal area weighting of the M3 Mean_Mean product, which is essentially what is derived from a tool such as Giovanni (the red symbols in Fig. 6). If we had chosen to forego the pixel threshold in the monthly grid calculations, we would have increased our monthly averages by ∼0.01 (#4). If we had no knowledge of pixel weighting, instead of deriving equal day averages at each grid (#2), we would have increased our values by nearly 0.05 over land and 0.03 over ocean. Applying only the daily pixel ($P > 5$) threshold (#3) yields similar results to simple (nonthreshold) pixel weighting (#4).

By keeping the same ordering of averaging, but instead of starting from the D3 QA_Mean product (#22), we would have decreased the result by 0.008 (to 0.249) over land but introduced no change to the result over ocean. If we derived a consistent confidence-weighted result (#23) from the QA_Mean, we would have reduced the over-land result by only −0.003 but increased over ocean by nearly 0.02 (to 0.202).

For May 2003, if the red symbols shown in Fig. 6 are considered to be our base case (#5), then taking the equal day average (or taking the average visually) of the blue points represents case #14. Over land, this estimate of the mean AOD would be larger by 0.04 (to 0.295). Over ocean, the increase is much less, only 0.003 (to 0.187). These two cases represent logical conclusions of using M3 (#5) versus using D3 (#14) data. If, instead, a user chose to describe the average from available L2 sampling (e.g., #18), then both over-land and over-ocean estimates would derive smaller results (than #5).

This article has been accepted for inclusion in a future issue of this journal. Content is final as presented, with the exception of pagination.

LEVY *et al.*: CRITICAL LOOK AT DERIVING MONTHLY AEROSOL OPTICAL DEPTH FROM SATELLITE DATA 11

TABLE I
GLOBAL MEAN AOD OVER LAND AND OCEAN DERIVED FROM DIFFERENT AGGREGATIONS OF TERRA-MODIS D3: MAY 2003

| | Averaging Order | Weighting Order | Land | Ocean | Equivalent to* |
|---|---|---|---|---|---|
| | | **From D3 Mean** | | | |
| 1 | Temporal then Spatial | Equal Day then Equal Cell | 0.320 | 0.222 | |
| 2 | Temporal then Spatial | Equal Day then Equal Area | 0.310 | 0.213 | |
| 3 | Temporal then Spatial | Equal Day (P>5) then Equal Area | 0.277 | 0.196 | |
| 4 | Temporal then Spatial | Pixel then Equal Area | 0.271 | 0.190 | |
| **5** | **Temporal then Spatial** | **Pixel (P>5) then Equal Area** | **0.257** | **0.184** | **M3 Mean_Mean: Equal Area Weighted** |
| 6 | Temporal then Spatial | Pixel (P>5 & Q≥1) then Equal Area | 0.251 | 0.185 | |
| 7 | Temporal then Spatial | Pixel then Pixel | 0.236 | 0.155 | |
| 8 | Temporal then Spatial | Pixel (P>5) then Pixel | 0.233 | 0.153 | |
| | | | | | |
| 9 | Spatial then Temporal | Equal Cell then Equal Day | 0.303 | 0.196 | |
| 10 | Spatial then Temporal | Equal Cell (P>5) then Equal Day | 0.272 | 0.176 | |
| 11 | Spatial then Temporal | Pixel then Equal Day | 0.236 | 0.155 | |
| 12 | Spatial then Temporal | Pixel (P>5) then Equal Day | 0.232 | 0.153 | |
| 13 | Spatial then Temporal | Pixel (P>5 & Q≥1) then Equal Day | 0.226 | 0.159 | |
| 14 | Spatial then Temporal | Equal Area then Equal Day | 0.295 | 0.187 | |
| 15 | Spatial then Temporal | Pixel then Pixel | 0.236 | 0.155 | |
| 16 | Spatial then Temporal | Pixel (P>5) then Pixel | 0.233 | 0.153 | M3 Mean_Mean: Pixel Weighted |
| | | | | | |
| 17 | Straight | Equal Cell | 0.304 | 0.196 | |
| 18 | Straight | Pixel | 0.236 | 0.155 | L2: Equal weighted |
| 19 | Straight | Pixel (P>5) | 0.233 | 0.153 | |
| | | **From D3 QA_Mean** | | | |
| 20 | Temporal then Spatial | Equal Day then Equal Cell | 0.302 | 0.221 | |
| 21 | Temporal then Spatial | Equal Day then Equal Area | 0.293 | 0.212 | |
| 22 | Temporal then Spatial | Pixel (P>5) then Equal Area | 0.249 | 0.184 | M3 QA_Mean_Mean: Equal Area Weighted |
| 23 | Temporal then Spatial | Confidence then Equal Area | 0.254 | 0.202 | |
| | | | | | |
| 24 | Spatial then Temporal | Equal Cell then Equal Day | 0.285 | 0.196 | |
| 25 | Spatial then Temporal | Confidence then Equal Day | 0.213 | 0.199 | |
| 26 | Spatial then Temporal | Equal Area then Equal Day | 0.278 | 0.188 | |
| | | | | | |
| 27 | Straight | Equal Cell | 0.286 | 0.196 | |
| 28 | Straight | Confidence | 0.213 | 0.200 | L2: Confidence weighted |

Blue/Red fonts represent minimum/maximum results from the aggregations presented over each surface.
**Bold** font indicates the "base" case explained in the text.
* Equivalent aggregation from other MODIS products (e.g. L2 or M3)

Estimates using #7 and #15 are equivalent to that using #18, as expected with consistent application of weighting. For the same reason, results of #8 and #16 are the same as that of #19 (confidence-weighted L2). Clearly, the choices made during the averaging process have a major impact on the results and must be properly documented.

Fig. 8 shows the 2003 time series for land and ocean separately, computed by some of the schemes listed in Table I (#2, #5, #14, #16, #18, #19, #21, #23, and #28). Aggregations of D3 products are indicated as small symbols with connecting lines, whereas aggregations of L2 or M3 are marked with large symbols. Equivalent aggregations are plotted with the same color and will have nearly overlapping symbols. For example, our base case time series, which is computed from the D3 Mean (#5; small open black squares), is equivalent to that computed from the M3 Mean_Mean (large black squares). We also see that, although the maximum AOD over both land and ocean seems to be in May, not all aggregations agree.
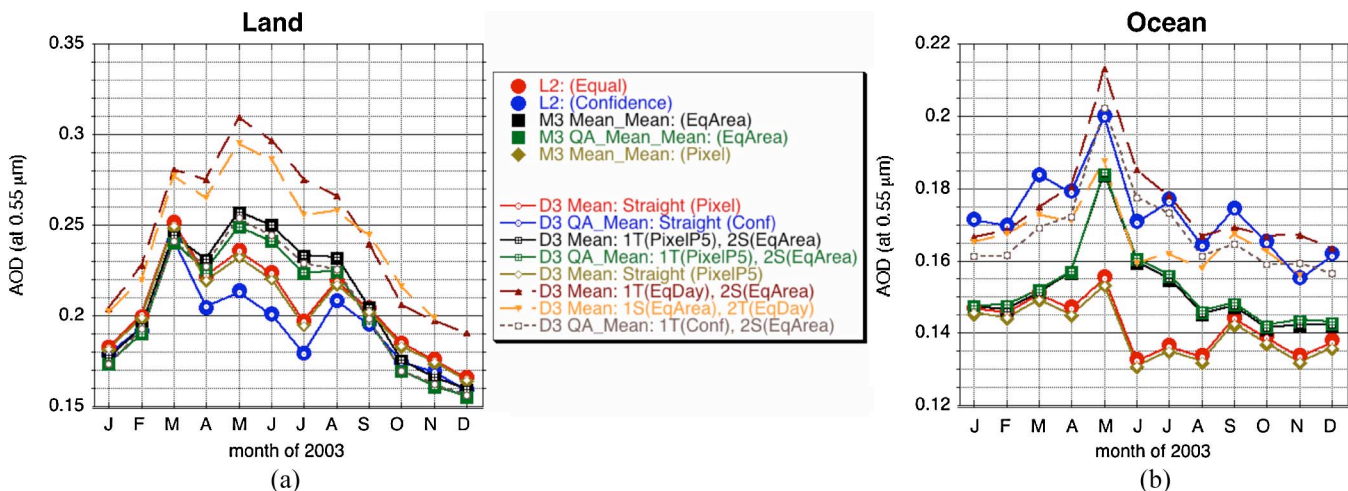
Fig. 8. Time series (Terra, 2003) of the monthly mean AOD computed from different aggregation/ordering/weighting methods over (a) land and (b) ocean. For each panel, values are computed from (large circles) L2, (large squares and diamonds) M3, and (small shapes and curves) D3. Each legend entry describes the type of averaging, including from which product the ordering and the weightings (in parentheses) are. For the ordering, they are listed by first (1) and second (2) and whether spatial (S) or temporal (T). Pairs of like colors (large shapes/small shapes) show equivalence. For example, "L2: (Confidence) " is equivalent to "D3 QA_Mean: Straight (Confidence)." The purple and orange triangles represent a case of reversing the spatial/temporal ordering.

Generally, the different aggregations derive a range of values for every month ($> 30\%$) that are similar to that discussed for May only (in Table I). Compared to our base case (black squares), choosing straightforward pixel weighting (red circles; e.g., (9) with $W = P$) derives similar or reduced mean AOD in all months over ocean but larger values during the fall and winter over land. Applying confidence weighting (blue circles) reduces the derived mean AOD over land by an additional 0.01–0.02 but tends to increase values over ocean. Over land, choosing to start from the D3 QA_Mean (green squares) rather than Mean leads to differences of about 0.01 for most months. Over ocean, the difference is negligible. Our consistent confidence weighting scheme (maroon triangles) gives results close to that of the current M3 product (QA_Mean_Mean; green) over land but higher values (by about 0.01) over ocean. Generally, the maximum monthly values are derived from temporal (with equal day weighting) then spatial (with equal area weighting) aggregation of the D3 Mean product (small maroon triangles).

Over land, QC tends to be lower over brighter surfaces near dust and biomass burning source regions, so that applying confidence weighting derives lower global mean values. Over ocean, QC tends to be higher where there is larger aerosol signal, so that applying confidence weighting derives higher values. We suspect that pixel weighting itself leads to lower values over the ocean because the clean SH ocean represents such a large percentage of the total ocean surface area (as well as the L2 sampling). On the other hand, the same region has lower confidence, so confidence weighting reduces its global impact on the global mean (making the result higher). Interestingly, comparisons with sun-photometer data show that the retrieved AOD values with QC = 1 are almost as accurate as those with QC = 3, so the best scheme is probably a combination of both pixel and confidence weightings.

Straightforward ordered pixel-weighted D3 with no daily PC threshold preserves L2 sampling (equivalence of red shapes). Similarly, straightforward confidence-weighted D3 preserves

L2 QA information (blue shapes). Because the M3 product assumes daily PC threshold, it does not represent the original L2. Nonetheless, based on our understanding of spatial and temporal homogeneity of AOD properties, this threshold ($P_{j,l} > 5$) seems to derive realistic gridded results without sacrificing much coverage. We believe that neither equal day weighting (with no thresholds; maroon) gives a realistic global mean over land nor straightforward confidence weighting (blue) is the answer, due to the subjectivity of the assigned QC. Although we cannot conclude that any averaging scheme is the correct one in all conditions, we believe that each one can provide insight into the "true" global statistics, and collectively, they can be used to help describe the uncertainty.

## VI. CONCLUSION

Global AOD is an inhomogeneous but not random physical property. It can exhibit large gradients, on scales ranging from tens of meters to hundreds of kilometers. Due to complications of orbital geometry, regions of persistent cloudiness, and other factors, satellite sampling varies greatly with season and location. Based on analysis of a specific year (2003) and month (May) of MODIS orbital (L2) and gridded (D3 and M3) AOD products, we have learned the following.

1) Pixel, confidence, equal cell, and equal area weightings, with or without PC or QA thresholds, are options for summarizing MODIS AOD. Straight pixel weighting exactly represents L2 sampling, whereas confidence weighting represents L2 confidence sampling. Applying a reasonable PC threshold ($P > 5$) screens regions with poor sampling statistics at the expense of reducing global coverage by 1%–2%.
2) Both standard monthly (M3) data products are pixel weighted and tend to provide similar results within a larger range of other aggregations.

This article has been accepted for inclusion in a future issue of this journal. Content is final as presented, with the exception of pagination.

LEVY *et al.*: CRITICAL LOOK AT DERIVING MONTHLY AEROSOL OPTICAL DEPTH FROM SATELLITE DATA 13

3) Different aggregation, weighting, and averaging-order choices can lead to very different regional and global average mean values.
4) Depending on the regionally varying relationship between AOD spatial gradients, clouds, and instrument sampling, different averages emphasize different attributes of the true aerosol field.
5) The ordering of spatial and temporal aggregation is non-commutative when data gaps are not accounted for in the weighting scheme.
6) The choice of averaging process will affect the interpretation of aerosol effects on climate.
7) The use of an exploratory tool like Giovanni shields the complexity of the data aggregation and should not be used exclusively for answering scientific questions.

Generally, application of either PC thresholds or pixel weighting tends to approximate L2 sampling. However, since MODIS L2 sampling is, by definition, biased toward clearer sky, as well as to darker surfaces, it is not necessarily representative of aerosol properties everywhere.

Compared to equal cell weighting, pixel weighting generally derives lower AOD over both land and ocean, because retrievals tend to be more abundant under clearer sky conditions. Applying confidence weighting tends to bias toward higher AOD over ocean and lower AOD over land, because there is often lower confidence in very low AOD retrievals over ocean, whereas over land, bright surfaces tend to produce lower confidence retrievals.

Satellite-retrieved aerosol products provide the means to characterize the global AOD field and estimate aerosol effects on climate. Yu *et al.* [7] calculate the (observationally based) aerosol DREs to be $-5.5 \pm 0.2$ and $-4.9 \pm 0.7 \, \text{W} \cdot \text{m}^{-2}$ over ocean and land, respectively. If we assume that DRE is linearly related to AOD (when AOD $\ll 1.0$) [26], then a global mean AOD error of 10% leads to an error of 10% on the DRE estimate. In a recent paper, Mishchenko *et al.* [27] pointed out that differences between different satellite's estimates of global DRE are more than 10%. Based on MODIS data, we showed that simply choosing different but otherwise reasonable averaging schemes can create differences that exceed 10% or even 30%. Thus, uncertainties in global AOD, and consequently, the uncertainty of DRE derived by a particular sensor may be greater in magnitude than differences among multiple sensors. This issue must be evaluated as part of any large-scale or long-term multi-satellite comparison.

We note that the standard D3 products (Mean and QA_Mean) are computed based on the assumption that the derived L2 AODs are normally distributed within the $1° \times 1°$ grid cell. However, it has been shown that global AOD demonstrates something closer to a lognormal probability distribution [28]. Consequently, one might consider deriving statistics based on the logarithms of the AOD within a grid box, which will likely result in a different value for the mean. Other assumptions of the distribution would lead to other values for the same area. It can be shown [29] that, in some areas, the difference may be several percent. However, even without the additional uncertainty of the AOD probability distribution, we showed here how different choices of aggregation, averaging, and weighting are capable of giving a wide range of results.

Clearly, more study is necessary to quantify how different averaging algorithms respond to sampling, confidence, clouds, and retrieval fitting errors, particularly on a regional basis. More generally, while beyond the scope of this paper, advanced spatial statistics techniques (e.g., [30]) could be applied to the L2 data to create new aerosol fields and uncertainty measurements based on the aggregate of available information.

Nonetheless, assessing the variability of different aggregations is key to understanding the uncertainty of satellite aerosol products for large-scale and long-time series applications. Depending on the regionally varying relationship between AOD spatial gradients, clouds, and instrument sampling, different averages will emphasize different attributes of the true aerosol field. Regional, rather than global, summaries will have advantages, in that they are likely to aggregate over fewer underlying spatial, temporal, and quality sampling differences.

## REFERENCES

[1] S. Solomon, D. Qin, M. Manning, Z. Chen, M. Marquis, K. B. Averyt, M. Tignor, and H. L. Miller, Eds., *Climate Change 2007: The Physical Science Basis. Contribution of Working Group I to the Fourth Assessment Report of the Intergovernmental Panel on Climate Change.* Cambridge, U.K.: Cambridge Univ. Press, 2007. 996 pp.

[2] T. L. Anderson, R. J. Charlson, D. M. Winker, J. A. Ogren, and K. Holmen, "Mesoscale variations of tropospheric aerosols," *J. Atmos. Sci.*, vol. 60, no. 1, pp. 119–136, Jan. 2003.

[3] L. A. Remer, Y. J. Kaufman, S. Mattoo, J. V. Martins, C. Ichoku, R. C. Levy, R. G. Kleidman, D. Tanré, D. A. Chu, R.-R. Li, T. F. Eck, E. Vermote, and B. N. Holben, "The MODIS aerosol algorithm, products, and validation," *J. Atmos. Sci.*, vol. 62, no. 4, pp. 947–973, Apr. 2005.

[4] R. A. Kahn, B. J. Gaitley, J. V. Martonchik, D. J. Diner, K. A. Crean, and B. Holben, "Multiangle Imaging Spectroradiometer (MISR) global aerosol optical depth validation based on 2 years of coincident Aerosol Robotic Network (AERONET) observations," *J. Geophys. Res.*, vol. 110, no. D10, p. D10 S04, Mar. 2005. DOI: 10.1029/2004JD004706.

[5] S. Kinne, M. Schulz, C. Textor, S. Guibert, Y. Balkanski, S. E. Bauer, T. Berntsen, T. F. Berglen, O. Boucher, M. Chin, W. Collins, F. Dentener, T. Diehl, R. Easter, J. Feichter, D. Fillmore, S. Ghan, P. Ginoux, S. Gong, A. Grini, J. Hendricks, M. Herzog, L. Horowitz, I. Isaksen, T. Iversen, A. Kirkevåg, S. Kloster, D. Koch, J. E. Kristjansson, M. Krol, A. Lauer, J. F. Lamarque, G. Lesins, X. Liu, U. Lohmann, V. Montanaro, G. Myhre, J. Penner, G. Pitari, S. Reddy, O. Seland, P. Stier, T. Takemura, and X. Tie, "An AeroCom initial assessment—Optical properties in aerosol component modules of global models," *Atmos. Chem. Phys.*, vol. 6, no. 5, pp. 1815–1834, Sep. 2006.

[6] M. I. Mishchenko, I. V. Geogdzhayev, W. B. Rossow, B. Cairns, B. E. Carlson, A. A. Lacis, L. Liu, and L. D. Travis, "Long-term satellite record reveals likely recent aerosol trend," *Science*, vol. 315, no. 5818, p. 1543, Mar. 2007. DOI: 10.1126/science.1136709.

[7] H. Yu, Y. J. Kaufman, M. Chin, G. Feingold, L. Remer, T. Anderson, Y. Balkanski, N. Bellouin, O. Boucher, S. Christopher, P. DeCola, R. Kahn, D. Koch, N. Loeb, M. S. Reddy, M. Schulz, T. Takemura, and M. Zhou, "A review of measurement-based assessments of aerosol direct radiative effect and forcing," *Atmos. Chem. Phys.*, vol. 6, no. 3, pp. 613–666, Feb. 2006.

[8] P. Hubanks, M. King, S. Platnick, and R. Pincus, *MODIS atmosphere L3 gridded product ATBD reference number: ATBD-MOD-30*, 2008. 91 pps. [Online]. Available: http://modis-atmos.gsfc.nasa.gov/reference_atbd.php

[9] J. G. Acker and G. Leptoukh, "Online analysis enhances use of NASA Earth science data," *EOS Trans. Amer. Geophys. Union*, vol. 88, no. 14, pp. 14–17, Jan. 2007.

[10] M. Steiner, T. L. Bell, Y. Zhang, and E. Wood, "Comparison of two methods for estimating the sampling-related uncertainty of satellite rainfall averages based on a large radar dataset," *J. Clim.*, vol. 16, no. 22, pp. 3759–3778, Nov. 2003.

[11] L. Zeng and G. Levy, "Space and time aliasing structure in monthly mean polar-orbiting satellite data," *J. Geophys. Res.*, vol. 100, no. D3, pp. 5133–5142, Mar. 1995.

This article has been accepted for inclusion in a future issue of this journal. Content is final as presented, with the exception of pagination.

14                                                                                                                  IEEE TRANSACTIONS ON GEOSCIENCE AND REMOTE SENSING

[12] S. A. Christopher and T. A. Jones, "Sample bias estimation for cloud-free aerosol effects over global oceans," *IEEE Trans. Geosci. Remote Sens.*, vol. 46, no. 6, pp. 1728–1732, Jun. 2008.

[13] G. Zhao and L. Di Girolamo, "Cloud fraction errors for trade wind cumuli from EOS-Terra instruments," *Geophys. Res. Lett.*, vol. 33, no. 20, p. L20 802, Oct. 2006. DOI: 10.1029/2006GL027088.

[14] T. A. Jones and S. A. Christopher, "Is the top of atmosphere dust net radiative effect different between Terra and Aqua?" *Geophys. Res. Lett.*, vol. 34, no. 2, pp. L02 812, Jan. 2007.

[15] J. Zhang and J. S. Reid, "MODIS aerosol product analysis for data assimilation: Assessment of over-ocean level 2 aerosol optical thickness retrievals," *J. Geophys. Res.*, vol. 111, no. D22, p. D22 207, Nov. 2006.

[16] N. Bellouin, A. Jones, J. Haywood, and S. A. Christopher, "Updated estimate of aerosol direct radiative forcing from satellite observations and comparison against the Hadley Centre climate model," *J. Geophys. Res.*, vol. 113, no. D10, p. D10 205, May 2008. DOI: 10.1029/2007JD009385.

[17] R. A. Kahn, M. J. Garay, D. L. Nelson, K. K. Yau, M. A. Bull, B. J. Gaitley, J. V. Martonchik, and R. C. Levy, "Satellite-derived aerosol optical depth over dark water from MISR and MODIS: Comparisons with AERONET and implications for climatological studies," *J. Geophys. Res.*, vol. 112, no. D18, p. D18 205, Sep. 2007.

[18] Y. J. Kaufman, L. A. Remer, D. Tanre, L. Rong-Rong, R. Kleidman, S. Mattoo, R. C. Levy, T. F. Eck, B. N. Holben, C. Ichoku, J. V. Martins, and I. Koren, "A critical examination of the residual cloud contamination and diurnal sampling effects on MODIS estimates of aerosol over ocean," *IEEE Trans. Geosci. Remote Sens.*, vol. 43, no. 12, pp. 2886–2897, Dec. 2005.

[19] L. A. Remer, D. Tanré, Y. Kaufman, R. Levy, and S. Mattoo, *Algorithm for Remote Sensing of Tropospheric Aerosol From MODIS: Collection 005*, Feb. 2009. Rev. 2, 97 pp. [Online]. Available: http://modis-atmos.gsfc.nasa.gov

[20] L. A. Remer, R. G. Kleidman, R. C. Levy, Y. J. Kaufman, D. Tanré, S. Mattoo, J. V. Martins, C. Ichoku, I. Koren, H. Yu, and B. N. Holben, "Global aerosol climatology from the MODIS satellite sensors," *J. Geophys. Res.*, vol. 113, no. D14, p. D14 S07, Jul. 2008. DOI: 10.1029/2007JD009661.

[21] R. C. Levy, L. Remer, S. Mattoo, E. Vermote, and Y. J. Kaufman, "Second-generation algorithm for retrieving aerosol properties over land from MODIS spectral reflectance," *J. Geophys. Res.*, vol. 112, no. D13, p. D13 211, 2007. DOI: 10.1029/2006JD007811.

[22] D. Tanré, Y. J. Kaufman, M. Herman, and S. Mattoo, "Remote sensing of aerosol properties over oceans using the MODIS/EOS spectral radiances," *J. Geophys. Res.*, vol. 102, no. D14, pp. 16 971–16 988, 1997.

[23] P. A. Hubanks, *MODIS Atmosphere QA Plan for Collection 005 Deep Blue Aerosol Update Version 3.5*, p. 61, 2007. [Online]. Available: http://modis-atmos.gsfc.nasa.gov/reference_atbd.php

[24] B. N. Holben, T. F. Eck, I. Slutsker, D. Tanre, J. P. Buis, A. Setzer, E. Vermote, J. A. Reagan, Y. J. Kaufman, T. Nakajima, F. Lavenu, I. Jankowiak, and A. Smirnov, "AERONET—A federated instrument network and data archive for aerosol characterization," *Remote Sens. Environ.*, vol. 66, no. 1, pp. 1–16, Oct. 1998.

[25] C. Ichoku, D. A. Chu, S. Mattoo, Y. J. Kaufman, L. A. Remer, D. Tanre, I. Slutsker, and B. N. Holben, "A spatio-temporal approach for global validation and analysis of MODIS aerosol products," *Geophys. Res. Lett.*, vol. 29, no. 12, p. 8006, Jun. 2002. DOI: 10.1029/2001GL013206.

[26] T. L. Anderson, R. J. Charlson, N. Bellouin, O. Boucher, M. Chin, S. A. Christopher, H. J. Haywood, Y. J. Kaufman, S. Kinne, J. Ogren, L. A. Remer, T. Takemura, D. Tanre, O. Torres, C. R. Trepte, B. A. Wielicki, D. Winker, and H. Yu, "An "A-Train" strategy for quantifying direct climate forcing by anthropogenic aerosols," *Bull. Amer. Meteorol. Soc.*, vol. 86, no. 12, pp. 1795–1809, Dec. 2005.

[27] M. Mishchenko, I. V. Geogdzhayev, B. Cairns, B. E. Carlson, J. Chowdhary, A. A. Lacis, L. Liu, W. B. Rossow, and L. D. Travis, "Past, present, and future of global aerosol climatologies derived from satellite observations: A perspective," *J. Quant. Spectrosc. Radiat. Transf.*, vol. 106, no. 1–3, pp. 325–347, Jul./Aug. 2007.

[28] N. T. O'Neill, A. Ignatov, B. N. Holben, and T. F. Eck, "The lognormal distribution as a reference for reporting aerosol optical depth statistics; Empirical tests using multi-year, multi-site AERONET sunphotometer data," *J. Geophys. Lett.*, vol. 27, no. 20, pp. 3333–3336, 2000.

[29] G. Leptoukh, S. Shen, J. G. Acker, and J. W. Campbell, *Statistical issues relevant to research use of Level 3 mapped ocean color data Products—Part 1: Comparisons of spatial averaging methods*, submitted for publication.

[30] N. Cressie and G. Johannesson, "Fixed rank kriging for very large spatial data sets," *J. R. Stat. Soc., Ser. B*, vol. 70, pt. 1, pp. 209–226, 2008.

**Robert C. Levy** received the B.A. degree in mathematics from Oberlin College, Oberlin, OH, in 1994, the M.S. degree in atmospheric science from Colorado State University, Fort Collins, in 1996, and the Ph.D. degree in atmospheric and oceanic science from the University of Maryland, College Park, in 2007.

Since 1998, he has been with Science Systems and Applications, Inc. (SSAI), Lanham, MD, working with the MODIS Aerosol Team at the NASA Goddard Space Flight Center, Greenbelt, MD. He has been increasingly responsible for upkeep, validation, and improvement of the MODIS aerosol algorithms over both land and ocean. In conjunction with his Ph.D. work, he developed a second-generation retrieval algorithm for deriving global aerosol over dark land. He is currently interested in using MODIS products to study relationships between aerosols, air quality, and climate.

**Gregory G. Leptoukh** received the M.S. degree in theoretical physics and the Ph.D. degree in cosmic ray physics from Tbilisi State University, U.S.S.R., in 1975 and 1985, respectively.

From 1976 to 1993, he did research in cosmic rays and high-energy physics with the Institute of Physics, Tbilisi, Georgia (formerly U.S.S.R.). From 1993 to 1996, he did research in physics with North Carolina State University, Raleigh. From 1996 to 1997, he was with NOAA/NESDIS. Since 1997, he has been with the NASA Goddard Space Flight Center, Greenbelt, MD, as a Contractor and then a Science Data Manager with the Goddard Earth Sciences Data and Information Services Center, where he provided science and data management support for various NASA Earth science missions. His current interests include multisensor and model data analysis and online analysis system development.

**Ralph Kahn** received the Ph.D. degree in applied physics from Harvard University, Cambridge, MA.

He is currently a Senior Research Scientist with the NASA Goddard Space Flight Center, Greenbelt, MD, where he is Aerosol Scientist for the NASA Earth Observing System's Multi-angle Imaging SpectroRadiometer (MISR). He focuses on using MISR's unique observations, combined with other data and numerical models, to learn about wildfire smoke, desert dust, volcano, and air pollution particles and to apply the results to regional and global climate-change questions. He has lectured on global climate change and atmospheric physics at the University of California, Los Angeles, and the California Institute of Technology, Pasadena. He is an Editor and the Founder of *PUMAS*, the online journal of science and math examples for precollege education.

**Viktor Zubko** received the M.S. degree in astrophysics (with honors) from Taras Shevchenko State University, Kiev, Ukraine, in 1979 and the Ph.D. degree in physics from the Main Astronomical Observatory, Ukrainian National Academy of Sciences, Kiev.

From 1997 to 1999, he was a Visiting Scientist with the Department of Physics, Technion–Israel Institute of Technology, Haifa, Israel. From 2000 to 2001, he was a Research Scholar with the Department of Physics and Astronomy, University of Kentucky, Lexington. From 2001 to 2004, he was a Research Scientist with NASA Goddard Space Flight Center (GSFC), Greenbelt, MD. From 2004 to 2006, he was a Senior Scientific Analyst with Nortel Government Solutions, Inc., Lanham, MD. He is currently an Atmospheric Scientist with Wyle Information Systems Group/Goddard Earth Sciences Data and Information Services Center, NASA GSFC. His experience includes theory and modeling of atmospheric aerosols and cosmic dust, polarized radiative transfer, light scattering by small particles, remote sensing of aerosols, numerical inversion techniques for ill-posed problems, principal component analysis, and scientific programming. He is currently researching the regional and temporal properties of atmospheric aerosols and developing scientifically justified methods and software for doing multisensor data fusion of geophysical parameters.

Dr. Zubko is a full member of the American Geophysical Union.

**Arun Gopalan** received the B.S. degree in mechanical engineering from the Victoria Jubilee Technical Institute, University of Mumbai, Mumbai, India, in 1991 and the M.S. degree from the NASA State University of New York, Stony Brook, in 1993.

He is currently a Research Scientist with Science Systems and Applications, Inc. (SSAI), Lanham, MD, working at the NASA Goddard Space Flight Center, Greenbelt, MD. His research interests include remote sensing data processing, retrieval algorithms, aerosol–cloud–climate feedback mechanisms, visualization of large Earth science data sets, and data mining.

**Lorraine A. Remer** received the B.S. degree in atmospheric science from the University of California, Davis, the M.S. degree in oceanography from the Scripps Institution of Oceanography, University of California, San Diego, and the Ph.D. degree in atmospheric science from the University of California, Davis.

She has been with the NASA Goddard Space Flight Center (GSFC), beginning in 1991, where she was with SSAI, Inc. until 1998, and a Civil Servant since then. She is currently a Physical Scientist with the Climate and Radiation Branch, Laboratory for Atmospheres, GSFC. She is a member of the EOS-MODIS Science Team and was a member of the Global Aerosol Climatology Project Science Team. Her current research interests include the climatic effects and remote sensing of atmospheric aerosol. She has been involved in several field campaigns including the Smoke/Sulfate, Cloud And Radiation (SCAR) experiments, the Tropospheric Aerosol Radiative Forcing Observational Experiment (TARFOX), the Israeli Desert Transition Zone experiment, the Puerto Rico Dust Experiment (PRiDE), and the Chesapeake Lighthouse Aircraft Measurements for Satellites (CLAMS).